Appl. Phys. A (2016) 122:497
DOI 10.1007/s00339-016-0025-8

Applied Physics A
Materials Science & Processing

TEA CO_2 laser machining of CFRP composite

A. Salama[1] · L. Li[1] · P. Mativenga[1] · D. Whitehead[1]

Received: 20 December 2015 / Accepted: 25 March 2016 / Published online: 11 April 2016

Abstract Carbon fibre-reinforced polymer (CFRP) composites have found wide applications in the aerospace, marine, sports and automotive industries owing to their lightweight and acceptable mechanical properties compared to the commonly used metallic materials. Machining of CFRP composites using lasers can be challenging due to inhomogeneity in the material properties and structures, which can lead to thermal damages during laser processing. In the previous studies, Nd:YAG, diode-pumped solid-state, CO_2 (continuous wave), disc and fibre lasers were used in cutting CFRP composites and the control of damages such as the size of heat-affected zones (HAZs) remains a challenge. In this paper, a short-pulsed (8 μs) transversely excited atmospheric pressure CO_2 laser was used, for the first time, to machine CFRP composites. The laser has high peak powers (up to 250 kW) and excellent absorption by both the carbon fibre and the epoxy binder. Design of experiment and statistical modelling, based on response surface methodology, was used to understand the interactions between the process parameters such as laser fluence, repetition rate and cutting speed and their effects on the cut quality characteristics including size of HAZ, machining depth and material removal rate (MRR). Based on this study, process parameter optimization was carried out to minimize the HAZ and maximize the MRR. A discussion is given on the potential applications and comparisons to other lasers in machining CFRP.

✉ A. Salama
adel.salama@postgrad.manchester.ac.uk;
afsalama405@yahoo.com

[1] Laser Processing Research Centre, School of Mechanical, Aerospace and Civil Engineering, The University of Manchester, Manchester M13 9PL, UK

1 Introduction

Composite materials such as CFRP composites have distinct advantages over conventional materials. CFRPs are gaining widespread uses in many applications where lightweight, high strength and corrosion resistance are essential, such as in the aerospace, automotive and marine industries [1]. Although the structures made by composites are often constructed and cured to the required shape, machining, such as trimming of the edges and drilling of assembly/fastening holes, remains unavoidable [2]. A carbon fibre-reinforced polymer consists of higher-strength abrasive fibres bonded within a weak polymer. This structure is heterogeneous and anisotropic depending on the constituent's physical properties, fibre orientation and laminar arrangement.

The inhomogeneity in the material properties and structures of CFRP composites makes their machining difficult by using mechanical, electrical discharge, abrasive water jet machining and lasers [3]. CFRP composites are more difficult to machine than conventional materials generally because they are heat sensitive and the carbon fibres are very abrasive [4]. Furthermore, the machining process can significantly affect these materials, leading to various forms of damages, such as delamination, fibres pull-out and heat damages. This can result in components being rejected at the last stage of their production sequence [5]. The main machining techniques used for CFRPs are mechanical cutting such as sawing, milling, drilling or grinding. Also, abrasive water jet (AWJ) cutting is used, due to its low tool wear and avoidance of heat-affected zone. Mechanical machining of CFRP composites often leads to excessive tool wear and delamination (e.g. Fig. 1) on fibre.

These result in an under-utilization of tools, as they have to be changed at low tool wear levels to control the process

Fig. 1 Fibre delamination of CFRP at the hole exit in a mechanically drilled hole

quality. These conditions increase machining time and cost. Abrasive water jet machining as an alternative processing technique yields good cut quality (no heat-affected zones) with lower tool wear than mechanical processing. However, such techniques need to cope with the water treatment, acoustic noise hazards and abrasive slurry disposal. In addition, they introduce moisture absorption and abrasive penetration of the cut surfaces [6]. Delamination and abrasive embedment between plies are also of major concern during AWJ machining of composites [7]. A laser as a focused, coherent beam of light has been widely used in various industrial applications for cutting and drilling due to its high speed, flexibility, ease of automation and being a non-contact process [8]. It offers several advantages, such as free of tool wear and contact force-induced problems [9]. However, as laser machining of CFRP composite is based on the interaction of a laser beam with at least two different materials with large material property differences, defects that are thermal in origin, such as HAZ, charring, matrix recession and delamination, are generated which are major obstacles in advancing laser machining of CFRP composites [3]. Among these defects HAZs may damage the structural properties of the composite materials [6]. Consequently, it is considered as a critical quality parameter in assessing the quality of the laser cutting of CFRP composites in this work. The large difference in thermal properties between the two constituent materials of CFRP composites results in excessive heat-affected zones [10]. This is considered as the major obstacle for wide industry applications of laser machining of CFRP composites. Minimizing or eliminating HAZ in the polymer matrix is a major challenge of laser processing of CFRP [7]. Since the HAZ is correlated with the laser-material interaction time, an approach to decrease it could involve the use of faster scanning speeds or shorter laser pulses. The release of high peak power in short time in pulsed laser mode results in quick evaporation of the material. This would reduce the heat absorbed by the matrix and hence limiting HAZ extension. Furthermore, the use of lasers in the pulsed mode allows for some cooling of the processed materials during the pulse-off time [11]. A TEA (transversely excited atmospheric pressure) CO_2 laser is a short-pulsed gas laser operating with a CO_2, N_2 and H_2 gas mixture at high pressures (1 atm or above) [12, 13] and produces higher peak powers (>100 kW) in short pulses (in the range of microseconds). The combination of high peak powers, short interaction time and good absorption of CO_2 wavelength by both matrix and fibres allows better coupling of the laser energy into the material, and thus, the heat damage could be reduced [7].

Except the machining of CFRP, the TEA CO_2 laser have been used in different fields of applications such as medical surgery [14], laser-material processing such as paint stripping, [15–17] and in non-destructive testing of composite materials in aerospace industry [18]. In contrast, considerable research work using other laser sources has been performed to investigate the laser processing of CFRP composite. Mathew et al. [2] used a Nd:YAG pulsed laser to identify and optimize the important parameters for machining of CFRP using a response surface methodology. These parameters include pulse energy, pulse duration, cutting speed, pulse repetition rate and gas pressure. The HAZ size achieved was between 0.5 and 2.4 mm. Herzog et al. [19] compared the effect of cutting on static strength of a CFRP laminate using a pulsed Nd:YAG laser, a disc laser and a continuous-wave CO_2 laser. They found that samples processed by the Nd:YAG laser had less HAZ and higher static and bending strengths. The HAZ sizes were in the range of 0.63–1.5 mm for all three lasers. Li et al. [20] used a diode-pumped solid-state UV laser to investigate the machining quality of CFRP. They showed that minimum HAZ (around 30–50 μm) can be obtained using a nanosecond pulsed UV laser. Negarestani et al. [10] developed a three-dimensional model to simulate the transient temperature field and subsequent material removal on a heterogeneous fibre–matrix mesh in laser machining of CFRP composite. They predicted the dimensions of the HAZ during laser machining of CFRP. The effect of laser parameters such as laser wavelength, power density, scanning speed and process gas on CFRP behaviour was studied by Negarestani and Li [21]. They also compared the laser machining process with other machining techniques such as mechanical and water jet techniques. The influence of processing parameters, in both continuous and pulsed-mode (millisecond) CO_2 laser, on the cut quality of CFRP was studied by Riverio et al. [22]. They found that the minimum heat-affected zone (0.54 mm) was obtained using CO_2 laser working in pulsed mode. Leone et al. [23] investigated the use of multi-passes

Table 1 Cutting quality (HAZ) of CFRP obtained with various laser types

Laser type	Wavelength	Machining condition	HAZ size	Refs.
Nd:YAG laser	1064 nm	Pulse energy 1.4–2.2 J Pulse length 0.2–1 ms Repetition rate 30–50 Hz	0.5–2.4 mm	[2]
Nd:YAG laser	1064 nm	Average power 300 W Peak power 18 kW Repetition rate 0.01–0.1 kHz	0.63–0.64 mm	[19]
Disc laser	1030 nm	Average power 3000 W Continuous wave	1.20–1.23 mm	
CO_2 laser	10.6 μm	Average power 500 W Repetition rate 0.1–20 kHz Quasi-continuous wave	1.34–1.50 mm	
Nd:YVO_4 laser	355 nm	Average power 10 W Pulse length 25 ns Repetition rate 40 kHz	0.05 mm	[20]
CO_2 laser	10.6 μm	Average power 300–3000 W Repetition rate 0.01–4 kHz Duty cycle 20–100 %	0.540–1.2 mm	[22]
Yb:YAG fibre laser	1064 nm	Average power 30 W Repetition rate 30–80 kHz Pulse length 50 ns Peak power 10–20 kW	0.1–0.25 mm	[23]
Nd:YAG	1064 nm	Average power 80 W Pulse length 10 ps Repetition rate 0.2–10 MHz	<5 μm	[25]

laser scanning technique in cutting of CFRP thin sheets using a 30-W MOPA Q-switched pulsed Yb:YAG fibre laser. They found that the kerf geometry was mainly affected by the scanning speed. Furthermore, the HAZ extent was influenced by the scanning speed as well as pulse power. Table 1 summarizes the cutting quality (HAZ) obtained with some laser types in processing of CFRP composites.

The large number of laser processing parameters necessitates the use of statistical modelling technique in order to understand the process parameter interactions. Mathew et al. [2] used response surface modelling (RSM) with central composite design (CCD) for experimental design and process parameter optimization of pulsed Nd:YAG laser cutting fibre-reinforced plastic composite sheet of 2 mm in thickness. The input factors were pulse energy, cutting speed, pulse duration, pulse repetition rate and gas pressure, while the output responses were HAZ and wall taper angle. Negarestani et al. [3] similarly performed a statistical analysis based on RSM and CCD to optimize the process parameters (pulse frequency, pulse energy and cutting speed) to improve the cut quality (fibre pull-out, taper angle and material remover rate) in nanosecond pulsed DPSS Nd:YAG laser cutting of CFRP composites with mixed reactive and inert gases. Negarestani et al. [24] also implemented, recently, statistical analysis based on RSM to optimize the process parameters during fibre laser cutting of carbon fibre-reinforced polymeric composites.

In the present work, TEA CO_2 laser machining of CFRP composite is reported for the first time. Design of experiments was used to understand the parameter interactions in the TEA CO_2 laser cutting of CFRP. These parameters include laser fluence, repetition rate and scanning speed. The effect of these parameters on the process behaviour including heat-affected zones, machining depth and material removal rate for the machining of CFRP was investigated.

2 Experimental methods

2.1 Design of experiments

Laser processing of material involves numerous parameters, which need to be optimized to achieve the required outcomes. The one-factor variation at a time approach commonly used requires a large number of runs and does not allow for the investigation of process variable interactions [26]. In order to tackle these difficulties the design of experiment statistical technique can be used. DOE is an

experimental-based modelling method involving the use of analytical techniques such as analysis of variance (ANOVA) to process the data and decide on individual and interaction factors that affect the process and their significances on process performance. Response surface modelling with CCD, Taguchi's method and factorial design are the most used DOE techniques in laser processing experiments. Ghosal and Manna [27] used RSM to develop comprehensive statistical models and optimize the machining parameters during laser machining of Al/Al_2O_3-MMC. Elmesalamy et al. [28] also employed the RSM based on CCD during ultra-narrow-gap laser welding of thick-section stainless steel to develop statistical models to understand the process parameter interactions and optimize the welding parameters. El-Taweel et al. [29] used Taguchi method to understand the effect of laser parameters on the cut quality during CO_2 laser cutting of Kevlar-49 composite and to determine the significant parameters and optimize the cutting parameters for better quality. Among these techniques RSM is a combination of mathematical and statistical techniques to correlate experimental responses with the input variables in mathematical models to optimize these responses. Moreover, the effect of variable interactions on responses can be graphically presented in a three-dimensional surface. Consequently, a Design Expert® software tool was used in this work for the experimental design using response surface methodology based on central composite design to show the effect of combinations of factors on behaviour of process responses and to develop mathematical models which relate the input laser variables (laser fluence, repetition rate and scanning speed) with the output responses (cross-sectional heat-affected zone, machining depth and material removal rate). Table 2 shows the input laser variables used and their levels. Six replications of centre runs were used for accurate estimation of the overall process errors. The selection of these operating parameter ranges was based on initial screening experiment to enable CFRP machining to take place. The fluence range was chosen to allow high ablation rates to be studied (Fig. 5).

2.2 Experimental procedure and materials

The laser cutting experiments was performed using Lumonics Impact 3150 HP TEA CO_2 laser system. The laser system specifications are listed in Table 3. The laser beam was delivered to the work piece by means of mirrors and focusing optics. An Aerotech computer-controlled X–Y CNC stage was used to traverse the workpieces. A multiple pass strategy was used during the machining. The schematic diagram of experimental setup is shown in Fig. 2. A square mask was used in the beam path before the focusing optics to select a uniform part of the laser beam and obtain a beam spot with sharp edges (Fig. 3b). A rectangular beam spot with a size of 0.9 mm by 0.9 mm obtained by passing the laser through a focussing lens (focal length 200 mm) was used in the experiment. This was used to reduce the heat-affected zone with a standard Gaussian beam geometry with large beam tapers (Fig. 3a).

The workpiece materials used for the studies were woven CFRP composite (Fig. 4a) of 80 mm long, 20 mm wide and 1.5 mm thick. The carbon fibre volume fraction was 55 %, and the matrix was epoxy resin. Experiments were performed to study the effect of laser process parameters, i.e. laser fluence, repetition rate and scanning speed on cross-sectional HAZ, machining depth and material removal rate. Each data point for all experimental responses was obtained by averaging the measured results for three measuring places along the length of laser machining.

The size of the cross-sectional HAZ (Fig. 4b) and laser machining quality were studied using optical microscopy. The material removal rate was calculated using:

$$\begin{aligned} \text{MRR} &= \frac{\text{Removed volume } (\text{mm}^3)}{\text{Process time } (\text{min})} \\ &= \frac{al}{\frac{nl}{v}} = \frac{av}{n} \end{aligned} \tag{1}$$

where a is measured cross-sectional area in mm^2, l is machined length in mm, v is scanning speed in mm/min, and n is number of machining passes.

3 Results

The effect of the number of laser pulses impinging the CFRP sample surface for three different laser fluences within low, intermediate and high range is shown in Fig. 5. A linear response of the ablation depth for an increasing of number of pulses can be clearly seen. The average ablation depth increased with the increase in the laser fluence, as expected. The ablation depth varied from 1.4 μm/pulse at

Table 2 Process variables and their levels

Symbol	Variable	Level 1	Level 2	Level 3	Level 4	Level 5
A	Fluence [J/cm^2]	60	69	83	96	105
B	Repetition rate [Hz]	37	60	94	127	150
C	Speed [mm/s]	20	35	58	80	95

Table 3 TEA CO_2 laser system specifications

Parameters	Specifications
Operating mode	Pulsed
Wavelength	10.6 μm
Maximum average power	300 W
Maximum pulse energy	2 J
Pulse repetition rate	up to 150 Hz
Pulse duration	8 μs, FWHM
Focal length	200 mm

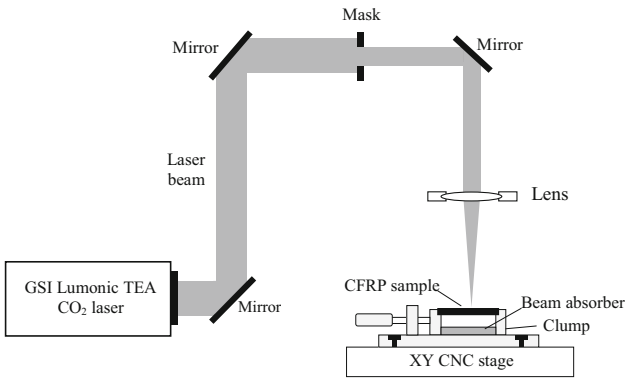

Fig. 2 Schematic diagram of experimental setup

low fluence (around 10 J/cm^2) to 8.3 μm/pulse at a high fluence (around 100 J/cm^2). The dependence of ablation rate on the laser fluence is shown in Fig. 6. R^2 and y in Figs. 5 and 6 are correlation coefficient and response variable (depth or ablation rate), respectively.

A threshold fluence of 3.1 J/cm^2, an absorption coefficient of 0.45 nm^{-1} and thermal loading of 14,703 kJ/cm^3 were determined using curve fitting and Eqs. (2) and (3) [30].

$$d = \frac{1}{\alpha}\ln\left(\frac{F}{F_{\text{th}}}\right) \tag{2}$$

where d the ablation rate, α the absorption coefficient (cm^{-1}), F the laser fluence (energy density) and F_{th} the threshold fluence. Moreover, the thermal loading γ (J/cm^3) of the CFRP can be calculated by:

$$\gamma = F_{\text{th}}.\alpha \tag{3}$$

3.1 Statistical models

The design matrix of process variables and the measured responses and the ANOVA tables for the responses obtained in this work are shown in "Appendix". Statistical empirical models with the best fit for the measured responses (cross-sectional HAZ, machining depth and MRR) were developed. To obtain the best-fit models, the suitability of proposed models were tested according to f value, lack of fit and ANOVA. The f value for a model is a comparative test between the term variance and the residual variance. It is the mean square for the term divided by the mean square for the residual. The Prob > f value of <0.05 for the model shows that the model terms are statistically significant, and values greater than 0.1 indicate that the model terms are not significant. Also the fitness of the developed models was examined by the regression coefficient $\acute{R}^2$ and adjusted $\acute{R}^2$ [28]. These values indicate the suitability of the RSM models. The models are more accurate if these values are closer to one. The $\acute{R}^2$ is the ratio of squares of the model to the sum of squares of the total. The adjusted $\acute{R}^2$ was calculated according to Eq. (4) [28].

$$\acute{R}^2_{\text{adj}} = \left(\frac{\acute{n}-1}{\acute{n}-p}\right)\left(1-\acute{R}^2\right) \tag{4}$$

where $\acute{n}$ is the number of experiments and p is the number of model parameters. In addition, the models of the responses were analysed by the normal plot of residuals and the residuals versus predicted chart (see "Appendix")

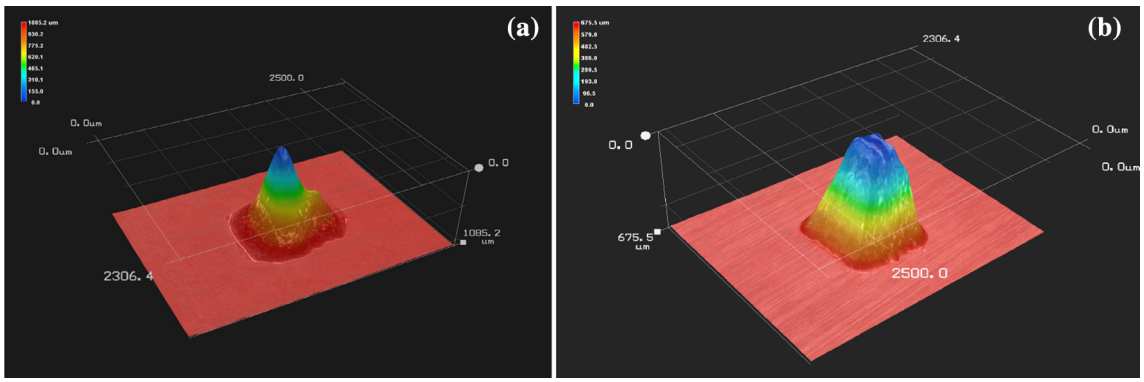

Fig. 3 TEA CO_2 laser beam profile; **a** without the projective mask, **b** with the projective mask

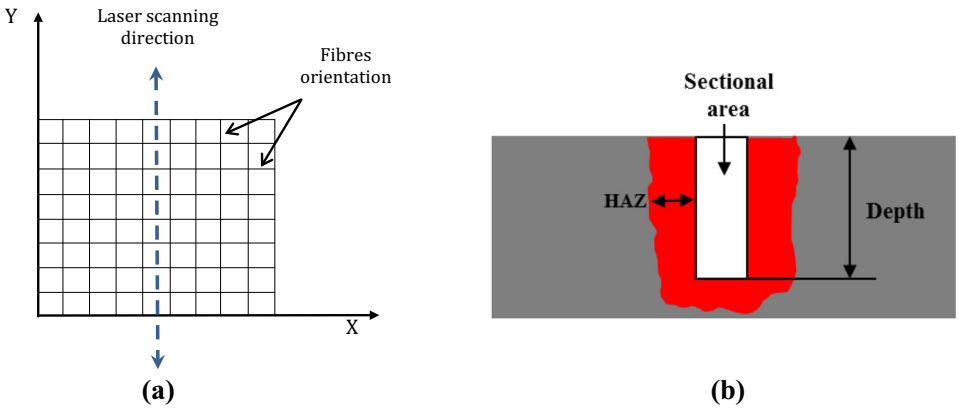

Fig. 4 Schematic view of **a** laser beam scanning direction and the woven fibre orientations, **b** quality features of a laser machined sample

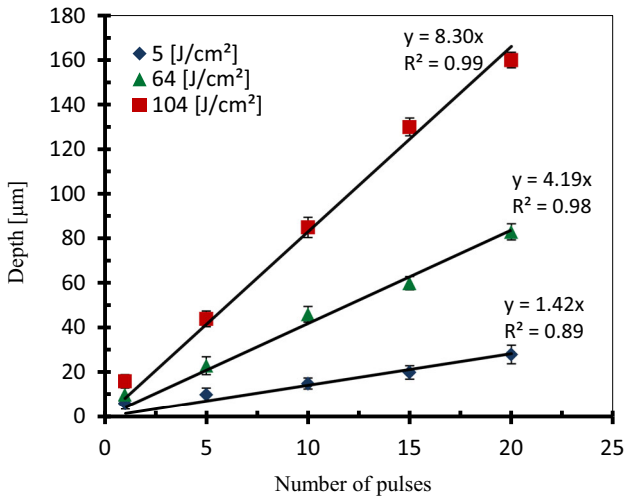

Fig. 5 Effect of number of laser pulses on the CFRP ablation depth for three different laser fluences

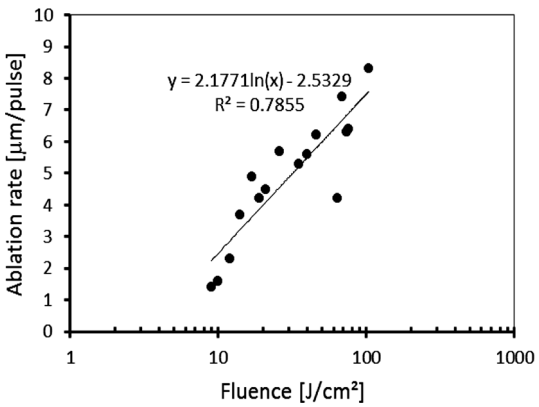

Fig. 6 Ablation rate dependence on laser fluence

to ensure the model suitability [31]. It can be seen from these plots that the points follow a normal distribution and the points scattered about the reference line. In order to optimize the response (η_r) and to analyse relationship between the response and the input variables (x_i and x_j) the general second-order polynomial Eq. (5) is usually used in RSM [32].

$$\eta_r = b_0 + \sum_{j=1}^{\acute{n}} b_j x_j + \sum_{j=1}^{\acute{n}} b_{jj} x_j^2 + \sum \sum_{i<j} b_{ij} x_i x_j \tag{5}$$

where b_0 is the responses at the centre point and b_i, b_{jj}, b_{ij} are the coefficients of linear, quadratic and interaction factors, respectively.

The ANOVA tables (see "Appendix") for cross-sectional HAZ, machining depth and MRR summarize the significant variables and the adequacy measures $\acute{R}^2$, adjusted $\acute{R}^2$ and predicted $\acute{R}^2$. The ANOVA tables show that the response models are significant and the lack of fit is insignificant. In addition, the "Adeq Precision" value which measures the signal-to-noise ratio indicates an adequate signal and the model can navigate the design space. A ratio greater than 4 is desirable. Therefore, the developed empirical models of cross-sectional HAZ, machining depth and MRR in terms of actual factors are shown in Eqs. (6)–(8) below.

$$\begin{aligned}\text{Cross sectional HAZ} = {} & 16.27 + 0.09 \times A + 0.31 \times B \\ & - 0.40 \times C - 1.69 \times 10^{-3} \times B^2 \\ & + 2.90 \times 10^{-3} \times C^2\end{aligned} \tag{6}$$

$$\begin{aligned}\text{Machining depth} = {} & -0.04 + 0.09 \times A + 0.08 \times B - 0.12 \\ & \times C - 9.97 \times 10^{-4} \times A \times C - 6.63 \\ & \times 10^{-4} \times B \times C + 1.55 \times 10^{-3} \times C^2\end{aligned} \tag{7}$$

$$\begin{aligned}\text{Material removal rate} = {} & -7.03 + 0.10 \times A + 0.1 \times B \\ & + 4.44 \times 10^{-3} \times C\end{aligned} \tag{8}$$

where A, B and C are fluence, repetition rate and scanning speed, respectively (dimensions shown in Table 2).

The statistical empirical models were compared with experimental results. The deviations were 1 μm for cross-sectional HAZ, 0.2 μm for the machining depth and 1 mm^3/min for the material removal rate.

3.2 Effect of process parameters on the machining responses

The effect of laser machining parameters and their interactions on the machining responses are presented in this section by considering perturbation graphs and 3D response surfaces for all responses.

3.3 Cross-sectional HAZ

Figure 7 is the perturbation plot that shows the effect of process parameters on the cross-sectional HAZ. It is apparent from this plot that the scanning speed is the most significant factor for HAZ. An increase in scanning speed can lead to a reduction of HAZ. It can also be observed from this figure that an increase of laser fluence increases the HAZ. The plot also shows minimum HAZ at low and high repetition rates. The relationships between all these process parameters are provided in Fig. 8. The values of cross-sectional HAZ range from 19 to 29 μm. It is clearly seen in Fig. 8a–c that reducing the laser fluence and increasing the scanning speed reduce the HAZ. The HAZ was minimum at lowest and highest repetition rate, whereas at middle value it was maximum. Figures 9 and 10 show the microscopic observations of the effect of lower and higher values of process variables on cross-sectional and top-surface HAZ, respectively. They show tapered cross sections, irregular wall shapes and top-surface burns.

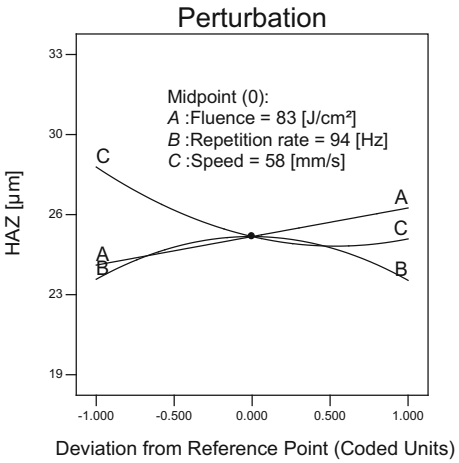

Fig. 7 Perturbation plot of effect of parameters on the cross-sectional HAZ

3.4 Machining depth

The perturbation plot in Fig. 11 shows the effect of laser parameters on machining depth. It shows that the scanning speed has the most significant effect on the machining depth. It is also observed that the machining depth increases by increasing the fluence and repetition rate, while decreasing with increases in the scanning speed. The response surface graphs presented in Fig. 12 show the effect of parameter interactions on the machining depth. It can be seen that the repetition rate and scanning speed interactions have a significant effect in which the highest machining depth can be obtained at a high repetition rate and a low scanning speed (Fig. 12c). It is also seen in Fig. 12a, b that the increase of laser fluence increases the machining depth. The effect of extreme values (low/high) of the process parameters on machining depth response is shown in Fig. 13.

3.5 Material removal rate

Figure 14 is a perturbation plot that shows the effect of laser fluence, repetition rate and scanning speed on MRR. It is observed that the repetition rate is the most effective parameter on MRR due to the high energy deposited per unit length at high repetition rate. The plot shows that the scanning speed has less effect on MRR compared with the other two parameters. The 3D surface response diagram in Fig. 15 shows the effect of parameter interactions on material removal rate. The MRR can be improved by increasing the repetition rate and laser fluence in Fig. 15a. It is also observed in Fig. 15b, c that the scanning speed has less effect on the MRR.

3.6 Optimization

The optimization of the responses was performed using numerical and graphical optimization by choosing the preferred goals for each variable and response. The statistical optimization performed based on the desirability function. The desirability function (Eq. 9) is the geometric mean of individual desirability ranging from zero for undesirable value to one for highest desirable value [31].

$$\xi = \left(\prod_{i=1}^{\acute{n}} d_i \right)^{\frac{1}{\acute{n}}} \tag{9}$$

where ξ is the overall desirability, $\acute{n}$ is the number of responses, and d_i is the ith response desirability value. The proposed solutions have the highest desirability depending on the responses obtained from the experiments. The desirability value "d_i" of individual responses is calculated as [33]:

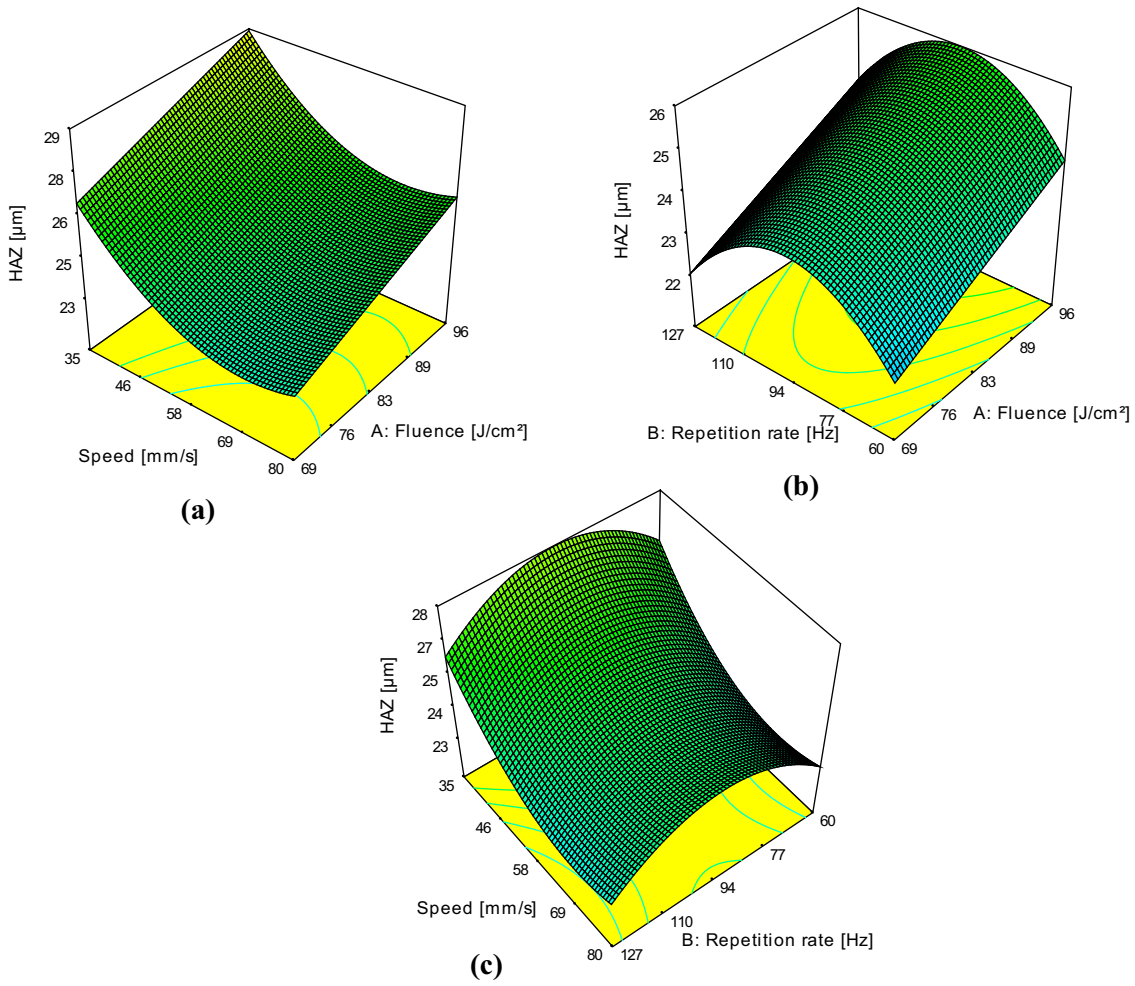

Fig. 8 Surface response graphs of cross-sectional HAZ model; **a** speed–fluence, **b** repetition rate–fluence, **c** speed–repetition rate

$$d_i = \begin{cases} \left[\dfrac{\acute{y} - \mathrm{A}}{\mathrm{B} - \mathrm{A}}\right]^{\mathrm{s}}, & A \le \acute{y} \le B \\ \left[\dfrac{\acute{y} - \mathrm{C}}{\mathrm{B} - \mathrm{C}}\right]^{\mathrm{t}}, & B \le \acute{y} \le C \end{cases} \tag{10}$$

where ý is the predicted response value; A, B and C are minimum, target and maximum response values, respectively; s and t are exponents that qualify the proximity of responses to the target value. The desirability varies from 0 to 1 according to the goal options (i.e. none, minimum, maximum, in range or target) and the response value $\acute{y}$, $d_i = 1$ if response value equals the target B, $di = 0$ if response value less than minimum value A and $0 < d_i > 1$ if the response value varies from minimum value A to maximum value C. The first part of Eq. (10) is used if maximized response is needed, whereas second part is used for minimization. The numerical optimization condition for all variables and responses is shown in Table 4, and the optimum numerical solution is shown in Table 5. The requirements in this work are to minimize cross-sectional HAZ, maximize machining depth and maximize the material removal rate. The highest importance was given to minimize the cross-sectional HAZ. The optimized operating window is shown in Fig. 16. The shaded region in the overlay plots is the region of the optimal working conditions that allow for selection of the optimum machining parameters. The overlay plot of graphical optimization is practically helpful for rapid determination of a process window among the numerous laser parameters values to achieve the required responses.

3.7 Optimum parameter validation

The predicted optimum numerical solution was validated experimentally. The average of three measured results were calculated and compared with predicted results. Table 6 summarizes the predicted values, experimental values and the deviation. The validation results show that the models

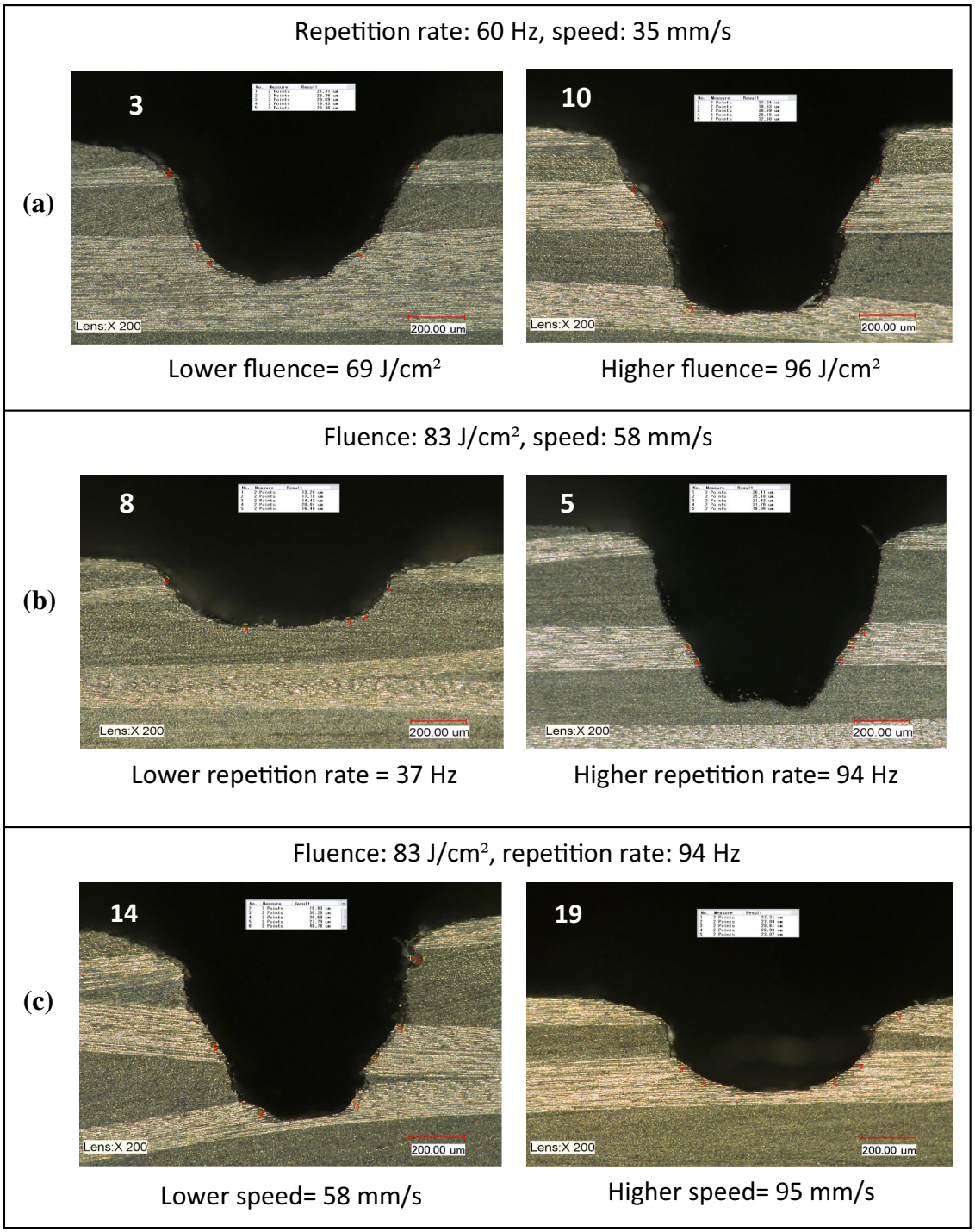

Fig. 9 Microscopic observations of cross-sectional view showing the effect of process parameters on cross-sectional HAZ; **a** fluence effect, **b** repetition rate effect, **c** speed effect. The *number* on each figure indicates the run number

developed are accurate and the deviations were in acceptable range. The standard deviations were considered for measurement errors. The microscopic observation quality of the machined sample using the optimum numerical solutions is shown in Fig. 17.

4 Discussion

The ANOVA results for cross-sectional HAZ indicate that the fluence, A, the scanning speed, C, and the quadratic terms B^2 and C^2 are significant terms. The increase of the

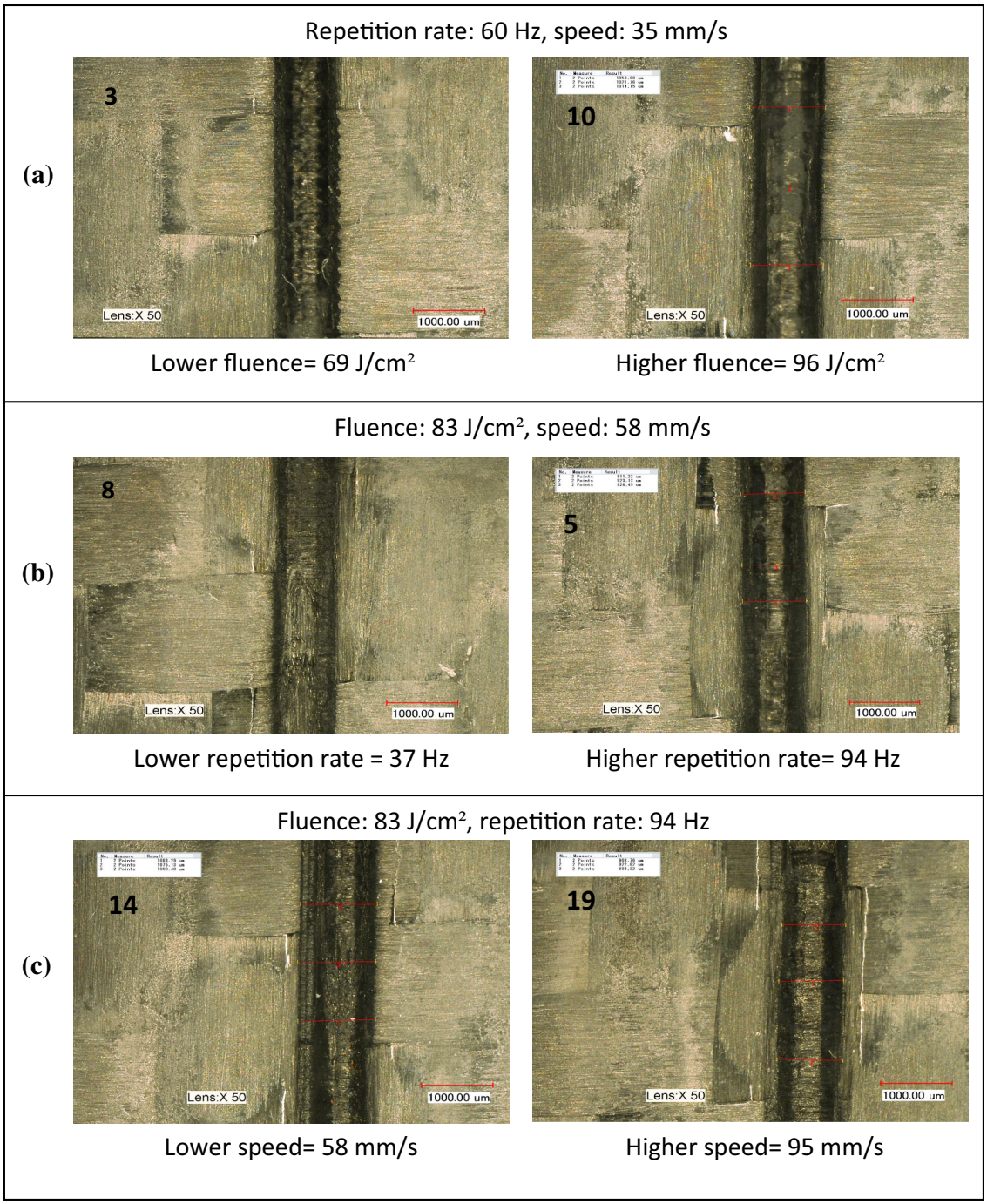

Fig. 10 Microscopic observations of top-surface view showing the effect of process parameters on top-surface HAZ; **a** fluence effect, **b** repetition rate effect, **c** speed effect. The *number* on each figure indicates the run number

heat input to the machining zone at high fluence results in a large HAZ. Moreover, reducing the scanning speed leads to long laser-material interaction time and high-pulse spot overlaps which create large HAZs. The higher is the scanning speed, the less the energy input per unite length to the materials and hence lower is the HAZ. At low-pulse repetition rates the pulse peak power is high enough to increase the machining ability, while giving time for the material to cool and therefore the material is removed with less heat spreading to the bulk materials. The reason for HAZ being reduced above certain value of repetition rate can be attributed to the reduction in pulse energy as the repetition rate was increased [34]. Furthermore, the drop of peak power at higher repetition rate

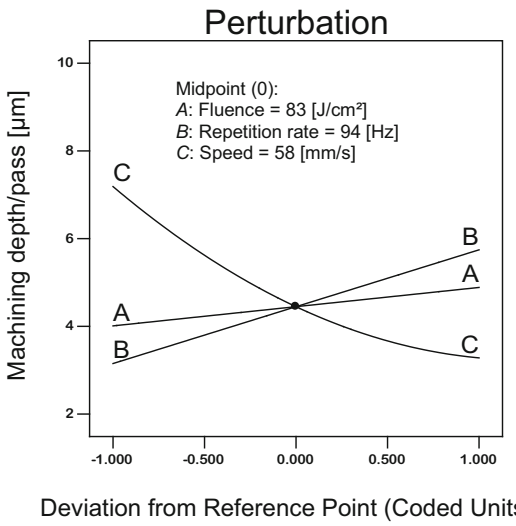

Fig. 11 Perturbation plot of effect of parameters on the machining depth

weakens the pulse and reduces the temperature on the machining zone [35].

The ANOVA table of machining depth reveals that the fluence, repetition rate, scanning speed, the interaction between fluence and speed, the interaction between repetition rate and scanning speed, the quadratic terms of scanning speed are the most significant terms affecting the machining depth. The effects of fluence, repetition rate and scanning speed in Fig. 12 indicate that high machining depth can be obtained at low scanning speed and high fluence and repetition rate. This is believed to be due to long laser-material interaction time at low scanning speed and high energy deposited to the machining zone due to large number of laser pulses.

The ANOVA of MRR indicates that repetition rates and laser fluences are significant terms, whereas the scanning speed has less effect compared to the repetition rate and fluence. The higher the repetition rate the higher the

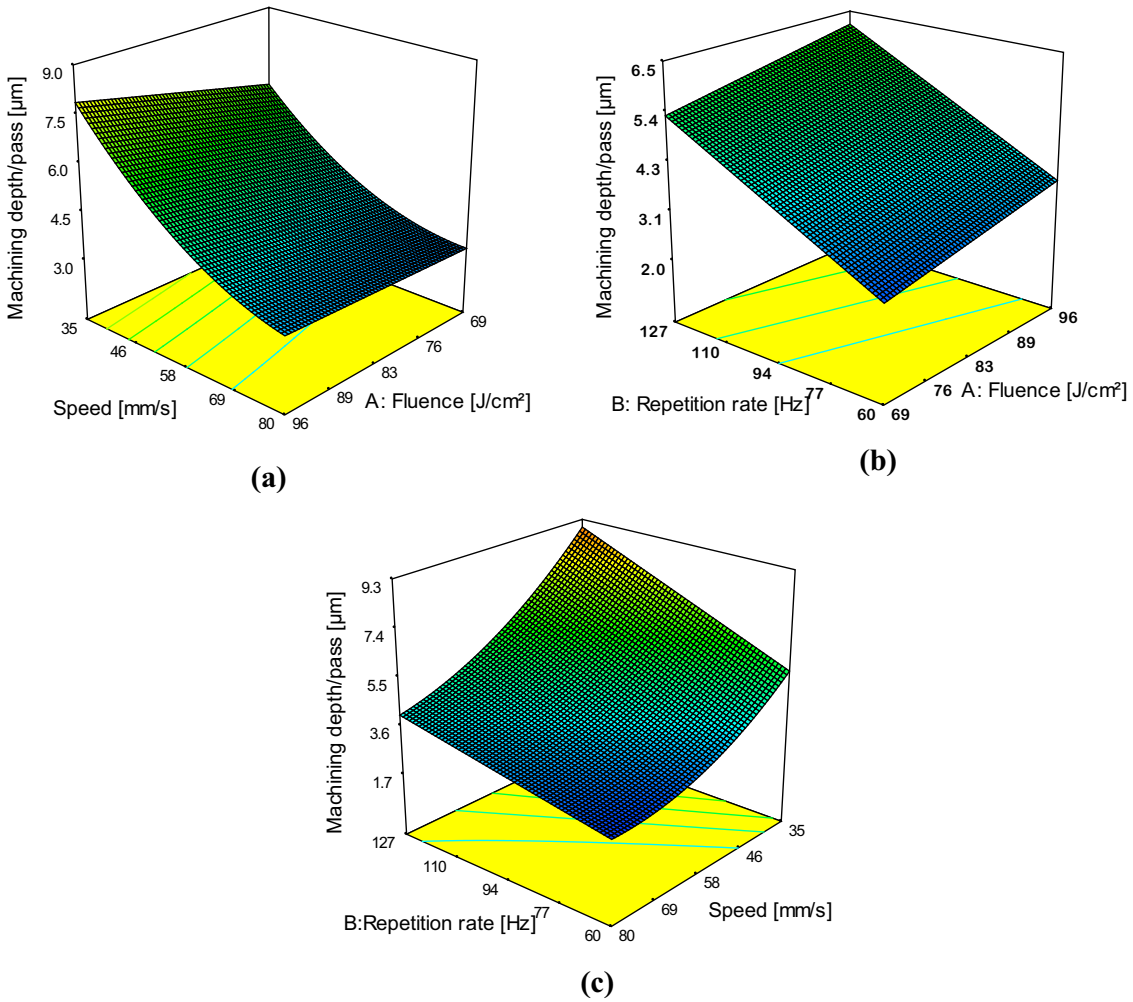

Fig. 12 Surface responses graph of the machining depth model; **a** speed–fluence, **b** repetition rate–fluence, **c** repetition rate–speed

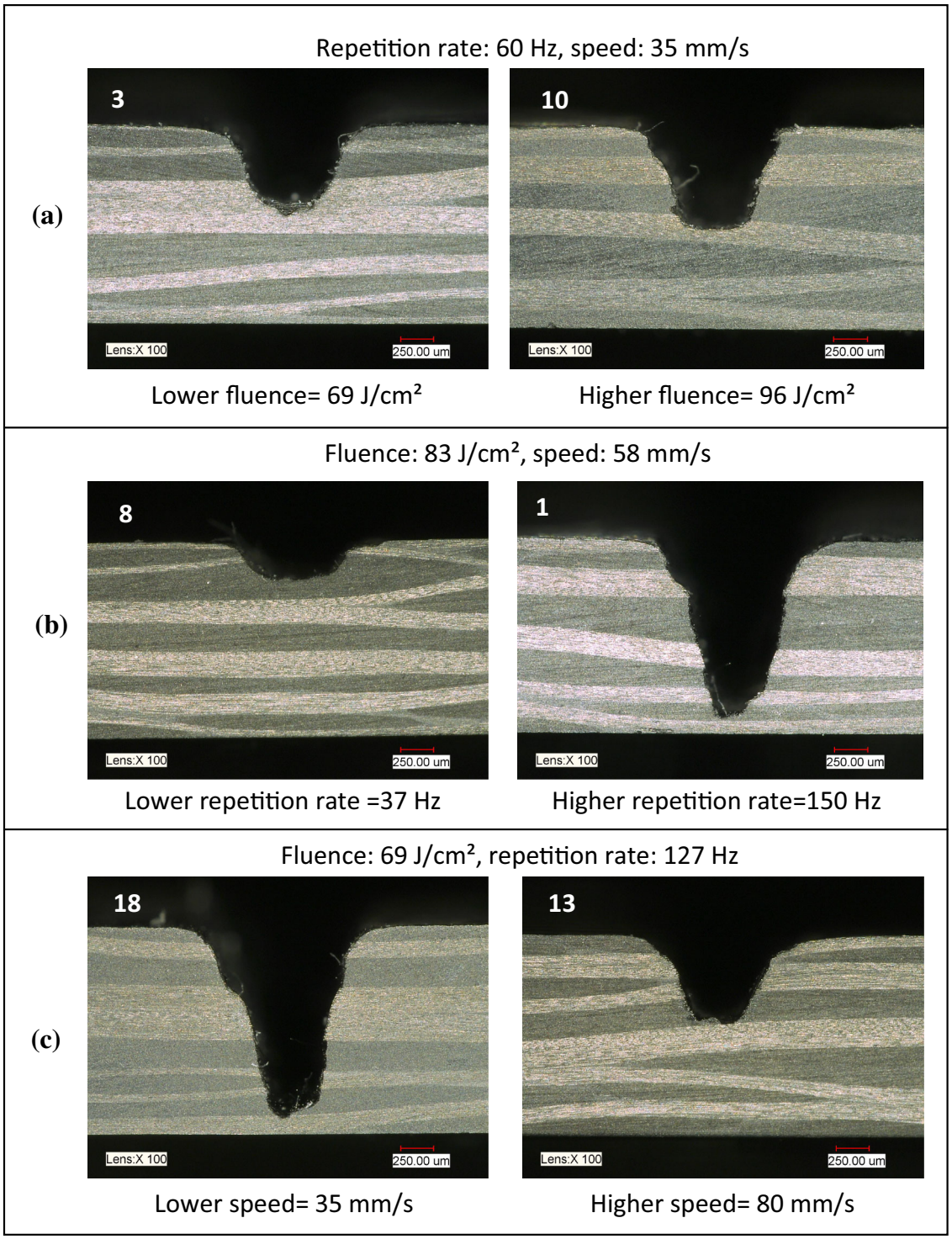

Fig. 13 Microscopic observation of cross-sectional view showing the effect of process parameters on machining depth; **a** fluence effect, **b** repetition rate effect, **c** speed effect. The *number* on each figure indicates the run number

number of pluses deposited into the machining zone and hence enhances the removal rate of materials. The increase of laser fluence widens the machining cross-sectional area and then improves the machining rate [2].

The microscopic observations of the cross sections in Figs. 9 and 13 show irregular shapes of the cross section. The difference in thermal properties between the carbon fibre and the epoxy matrix and the nature of the

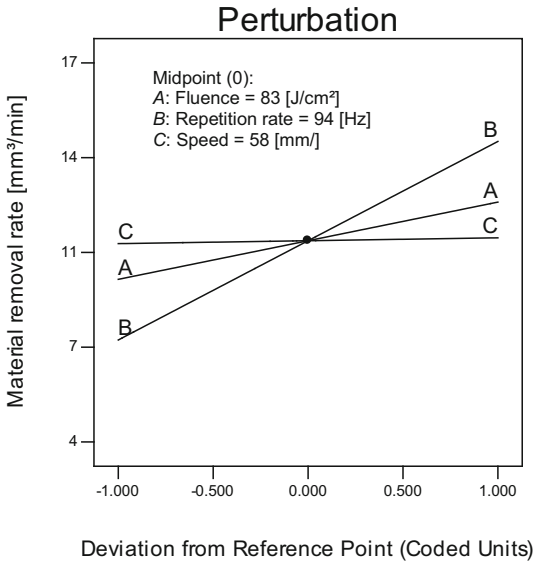

Fig. 14 Perturbation plot of effect of parameters on the material removal rate

material composition (parallel and perpendicular fibre direction to laser motion) make the cross section not smooth. This could be attributed to the difference in thermal conductivity of the carbon fibre in axial and radial directions (higher in axial direction than radial) also to the low thermal conductivity of the matrix, i.e. 50 W/m.K for carbon fibre and 0.1 W/m.K for epoxy [21]. In the areas where the fibres were parallel to the laser motion the kerf was wider. In these areas the heat conducted away along the fibres and work to preheat the material ahead of the laser beam. This can enhance the energy existing in these areas, due to less heat conduction in radial direction, and leads to more material removal, whereas when the fibres were perpendicular to the laser motion the efficiency of the process reduced due to the loss of the generated heat from the machining zone by conducting away through fibres leading to reduction in the cross section [36].

In addition to the irregular cut section, the cross-sectional views show taper walls of the cut in which the kerf

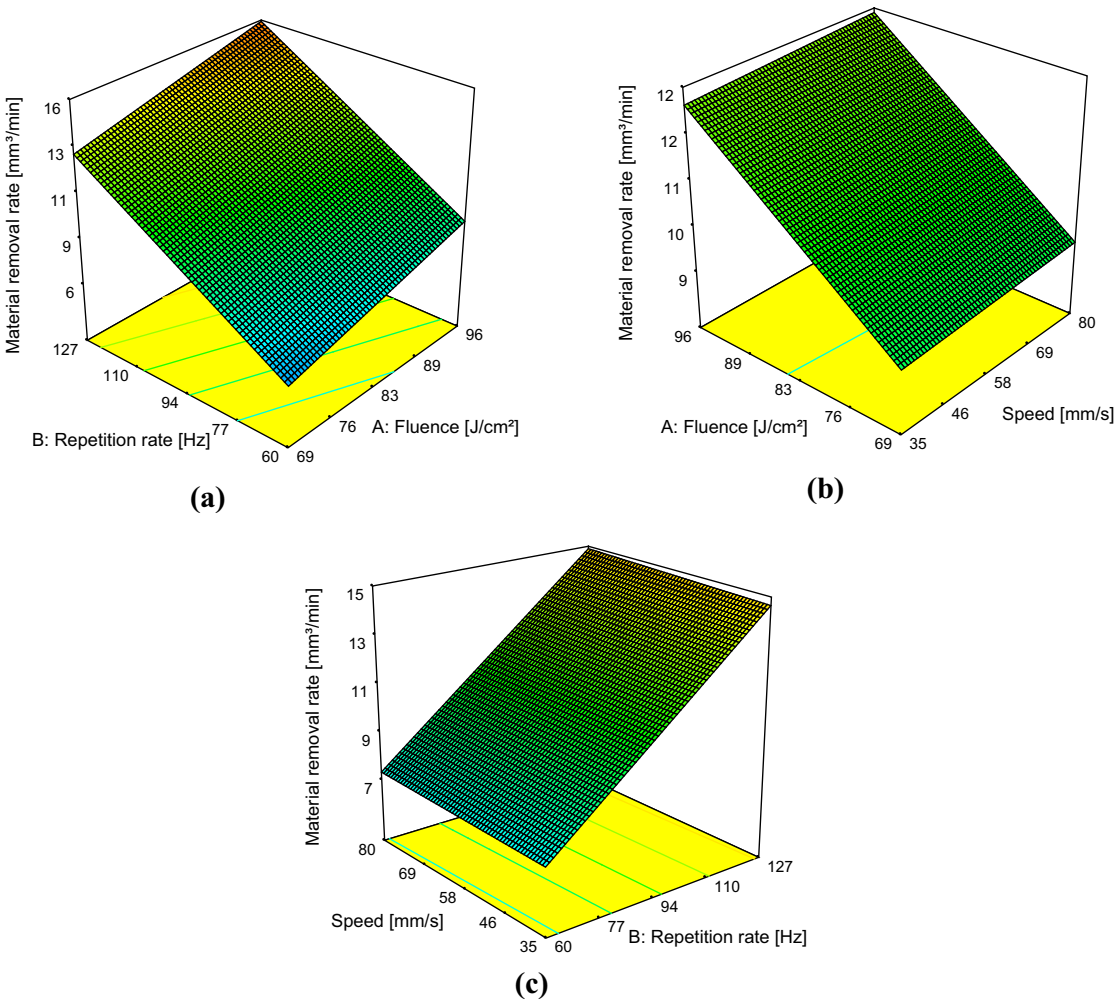

Fig. 15 Surface response graphs of material removal rate model; **a** repetition rate–fluence, **b** fluence–speed, **c** speed–repetition rate

Table 4 Numerical optimization condition

Variable and response	Goal	Lower limit	Upper limit	Importance
Fluence [J/cm^2]	In range	69	105	3
Repetition rate [Hz]	In range	60	127	3
Speed [mm/s]	In range	35	95	3
HAZ [μm]	Minimize	19	33	5
Machining depth [μm]	Maximize	1.6	10	3
Material removal rate [mm^3/min]	Maximize	4	17	3

Table 5 Optimum numerical solution

No	Fluence [J/cm^2]	Repetition rate [Hz]	Speed [mm/s]	HAZ [μm]	Machining depth [μm]	Material removal rate [mm^3/min]	Desirability
1	69	127	46	23	6.5	13	0.70

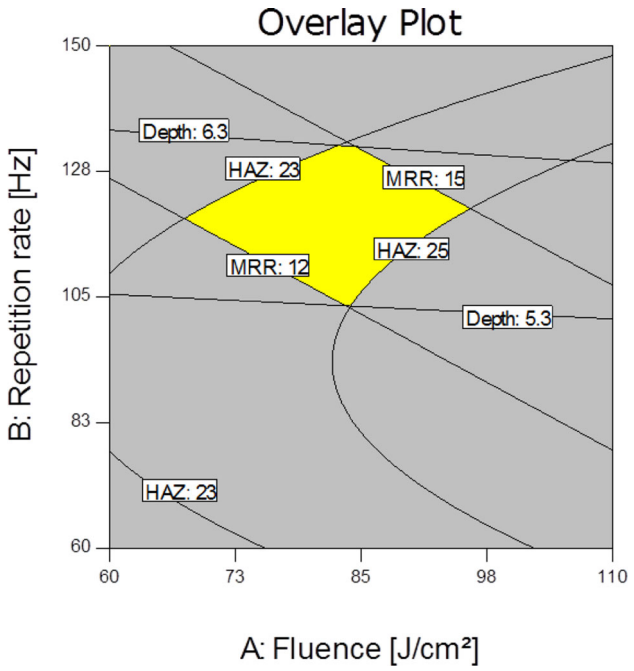

Fig. 16 *Overlay plot* shows the optimal working region where the *yellow zone* is the optimized process window. The HAZ plotted is the cross-sectional HAZ

width reduced as the machining depth increases. The reduction of the kerf width at the bottom could be due to the side wall absorption of the laser beam resulting in less laser energy at the kerf bottom, thereby reducing the kerf width [37]. Moreover, the reduction of the laser energy absorbed by the material as the depth increases due to plasma/plume scattering of the laser beam and the reduction of energy density due to the laser beam divergence after the focal point is another reason for the tapering [2].

The top-surface charring shown in Fig. 10 is related to the nature of the surface (glossy surface) and beam shape (Fig. 3b) in which higher power density is at the beam centre and reduced away from the centre, also due to the plasma and ejected vapour generated which reheat the top surface and causes high thermal damage. On the contrary, little HAZ is shown at the middle of cross section along the fibre perpendicular to the cut path. This could be due to less heat localized. In Fig. 17, some de-bounded fibres are shown at the bottom surface where the fibre direction is parallel to the cutting path. Referring to what mentioned before, less laser energy reaching the kerf bottom and the localized heat at this region are enough to remove some of the carbon fibres but high enough to vaporize the epoxy matrix leaving some de-bonding fibres.

The improved quality obtained using TEA CO_2 laser is attributable to the high absorptivity of the carbon fibres and the matrix to the CO_2 wavelength of 10.6 μm, where the laser radiations are absorbed simultaneously by both the carbon fibre and polymer making effective disintegration of polymer much more easily. The advantage of that is that polymer can disintegrate more quickly. This makes the TEA CO_2 laser different from other lasers such as YAG

Table 6 Predicted values, experimental values and the deviation

Responses	HAZ [μm]	Machining depth [μm]	Material removal rate [mm^3/min]
Predicted results	23	6.5	13
Experimental results	21 ± 4	5.8 ± 0.3	11 ± 0.4
Deviation	1	0.2	1

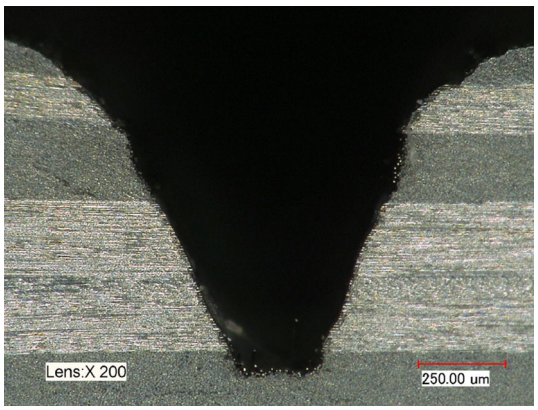

Fig. 17 Cross-sectional view of the machined sample for optimum solution

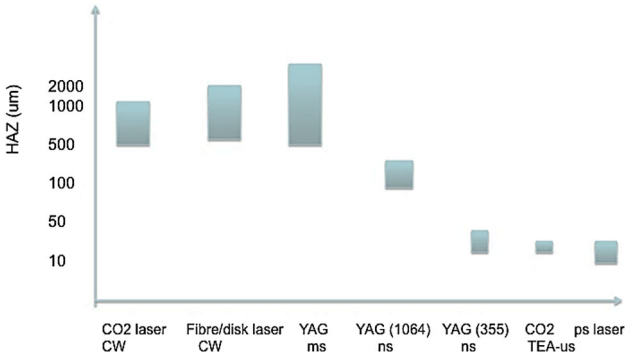

Fig. 18 Comparison of the effect of different lasers and machining methods on HAZ (CW means continuous wave)

(1064 nm) and Yb-fibre laser (1070 nm) where the laser is mainly absorbed by the carbon fibre and is normally transparent to polymer. These near-IR lasers heat the carbon fibre, and the heat is conducted from the carbon fibre to the polymer; thus, it is less affective and generates larger heat-affected zones [7, 38]. Furthermore, the high peak power of TEA CO_2 laser (250 kW) released on a short time results in rapid ablation of the CFRP composite leaving little time for the heat to propagate to the surrounding materials, and the cooling time between the pulses further improves the machining equality. Figure 18 compares and summarizes the heat-affected zone generation using laser cutting machining methods. It is clear from the figure that shorter pulses would enable better quality cutting for CFRPs. The current state of the art shows the capability of laser machining to achieve HAZ within tens of micrometres.

The TEA CO_2 laser machining of CFRP shows better quality and low machining rate than those obtained using continuous CO_2, fibre and Nd:YAG lasers [3, 39], whereas it is showing inferior quality than those obtained using femtosecond and picosecond lasers, but its machining rate is higher than fs and ps lasers [25]. The highly efficient and low operating cost [40, 41], better quality compared with CW CO_2, fibre and YAG lasers and higher machining rate than picosecond laser make the TEA CO_2 laser potentially a practical tool for scarf repair of CFRP composite, acoustic hole drilling, edge trimming applications. Furthermore, since TEA CO_2 lasers with an average power of more than 1 kW have become available [17], practical use of TEA CO_2 lasers for machining CFRP composite may become economically and practically viable.

5 Conclusions

This paper presented pulsed TEA CO_2 laser machining of carbon fibre-reinforced polymer composites for the first time. The influence of laser fluence, repetition rate and scanning speed on cross-sectional heat-affected zone extension, machining depth and material removal rate has been investigated using design of experiment. Statistical empirical models of the responses and the significant process parameters among selected parameters were developed in this work. From this work, the following conclusions can be drawn:

1. The TEA CO_2 laser shows good machining quality (cross-sectional HAZ) of CFRP composite. The optimum machining results achieved for average cross-sectional HAZ, machining depth and material removal rate were 21 ± 4 μm, 5.8 ± 0.3 μm/pass and 11 ± 0.4 mm^3/min, respectively.
2. The HAZ was significantly affected by the laser fluence, scanning speed, square of repetition rate and square of scanning speed.

Appendix

The design matrix of process variables and the measured responses, ANOVA tables of the responses and the diagnostic plots are shown below:

See Tables 7, 8, 9, 10 and Fig. 19.

Table 7 Design matrix of process variable and measured responses

Run	Variables			Responses		
	Fluence [J/cm^2]	Repetition rate [Hz]	Speed [mm/s]	HAZ [μm]	Machining depth [μm]	MRR [mm^3/min]
1	83	150	58	20	6.7	15
2	60	94	58	21	3.7	8
3	69	60	35	24	4.6	6
4	83	94	58	23	4.8	10
5	83	94	58	24	4.3	12
6	96	127	80	22	4.4	14
7	83	94	20	33	10.0	9
8	83	37	58	19	2.0	4
9	83	94	58	27	4.9	12
10	96	60	35	29	5.1	8
11	83	94	58	25	4.7	13
12	83	94	58	29	3.9	12
13	69	127	80	23	3.8	13
14	83	94	58	27	4.4	12
15	96	127	35	28	9.6	17
16	96	60	80	26	2.7	8
17	105	94	58	24	5.2	14
18	69	127	35	25	9.0	13
19	83	94	95	25	3.3	11
20	69	60	80	24	2.5	7

Table 8 ANOVA for the cross-sectional HAZ (*df* degrees of freedom)

Source	Sum of squares	*df*	Mean squares	*f* value	Prob > f	
Model	146.43	5	29.29	5.17	0.0068	Significant
A—fluence	21.27	1	21.27	3.76	0.0731	
B—repetition rate	7.4E−003	1	7.4E−003	1.3E−003	0.9717	
C—speed	33.70	1	33.70	5.95	0.0286	
B^2	52.06	1	52.06	9.19	0.0090	
C^2	31.34	1	31.34	5.53	0.0338	
Residual	79.32	14	5.67			
Lack of fit	54.48	9	6.05	1.22	0.4353	Not significant
Pure error	24.83	5	4.97			
Cor total	225.75	19				
Standard deviation = 2.38					$\acute{R}^2 = 0.65$	
Mean = 24.75					Adjusted $\acute{R}^2 = 0.52$	
Coefficient of variation = 9.62					Predicted $\acute{R}^2 = 0.31$	
Predicted residual error of sum of squares (PRESS) = 156.77					Adequate precision = 9.34	

Table 9 ANOVA for the machining depth

Source	Sum of squares	*df*	Mean squares	*f* value	Prob > f	
Model	89.44	6	14.91	205.78	<0.0001	Significant
A—fluence	2.62	1	2.62	36.22	<0.0001	
B—repetition rate	22.95	1	22.95	316.82	<0.0001	
C—speed	52.08	1	52.08	718.83	<0.0001	
AC	0.72	1	0.72	9.94	0.0076	
BC	2.00	1	2.00	27.61	0.0002	
C^2	9.07	1	9.07	125.24	<0.0001	
Residual	0.94	13	0.07			
Lack of fit	0.24	8	0.03	0.22	0.9722	Not significant
Pure error	0.70	5	0.14			
Cor total	90.39	19				
Standard deviation = 0.27					$\acute{R}^2 = 0.99$	
Mean = 4.99					Adjusted $\acute{R}^2 = 0.98$	
Coefficient of variation = 5.40					Predicted $\acute{R}^2 = 0.98$	
Predicted residual error of sum of squares (PRESS) = 1.59					Adequate precision = 48.28	

Table 10 ANOVA for the material removal rate

Source	Sum of squares	*df*	Mean squares	*f* value	Prob > f	
Model	182.29	2	91.14	60.74	<0.0001	Significant
A—fluence	23.96	1	23.96	15.97	0.0009	
B—repetition rate	158.33	1	158.33	105.51	<0.0001	
Residual	25.51	17	1.50			
Lack of fit	20.68	12	1.72	1.78	0.2157	Not significant
Pure error	4.83	5	0.97			
Cor total	207.80	19				
Standard deviation = 1.22					$\acute{R}^2 = 0.88$	
Mean = 10.90					Adjusted $\acute{R}^2 = 0.86$	
Coefficient of variation = 11.24					Predicted $\acute{R}^2 = 0.83$	
Predicted residual error of sum of squares (PRESS) = 34.86					Adequate precision = 24.14	

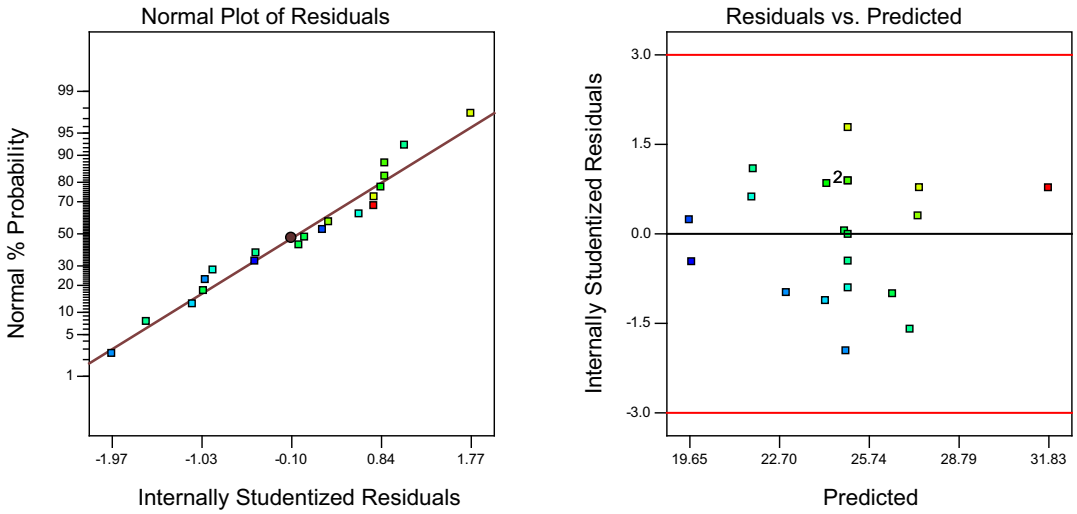
Normal Plot of Residuals
Normal % Probability
99
95
90
80
70
50
30
20
10
5
1
-1.97
-1.03
-0.10
0.84
1.77
Internally Studentized Residuals
Residuals vs. Predicted
Internally Studentized Residuals
3.0
1.5
0.0
-1.5
-3.0
2
19.65
22.70
25.74
28.79
31.83
Predicted

(a)

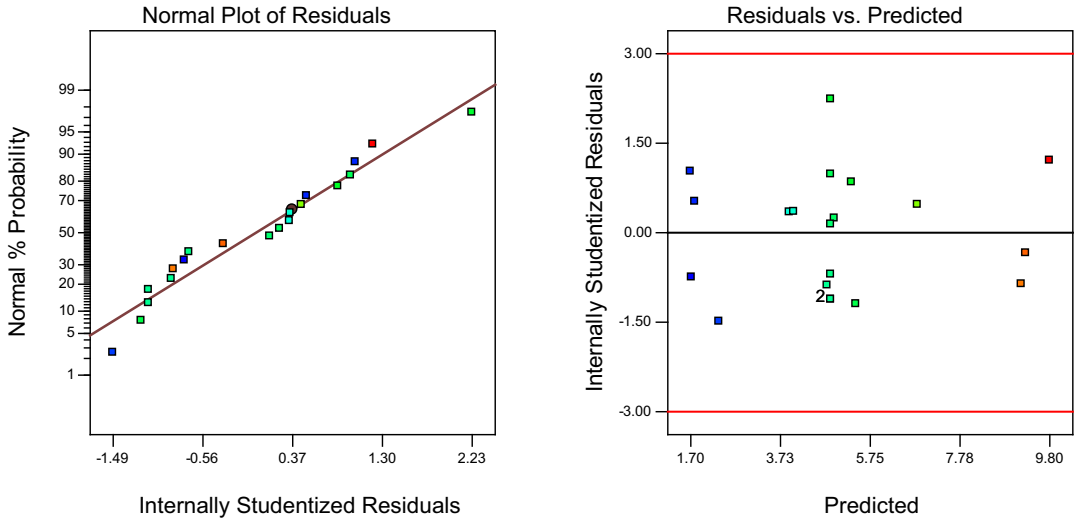
Normal Plot of Residuals
Normal % Probability
99
95
90
80
70
50
30
20
10
5
1
-1.49
-0.56
0.37
1.30
2.23
Internally Studentized Residuals
Residuals vs. Predicted
Internally Studentized Residuals
3.00
1.50
0.00
-1.50
-3.00
2
1.70
3.73
5.75
7.78
9.80
Predicted

(b)

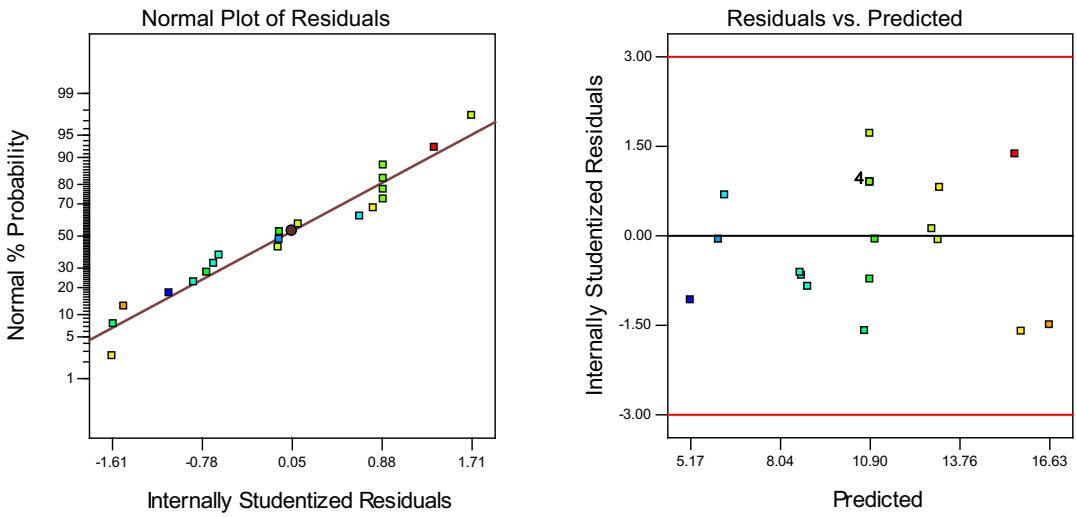
Normal Plot of Residuals
Normal % Probability
99
95
90
80
70
50
30
20
10
5
1
-1.61
-0.78
0.05
0.88
1.71
Internally Studentized Residuals
Residuals vs. Predicted
Internally Studentized Residuals
3.00
1.50
0.00
-1.50
-3.00
4
5.17
8.04
10.90
13.76
16.63
Predicted

(c)

◄**Fig. 19** Diagnostic plots of normal plot of residuals and residual versus predicted values for: **a** cross-sectional HAZ, **b** machining depth and **c** MRR

References

1. K.T. Voisey, S. Fouquet, D. Roy, T.W. Clyne, Opt. Laser. Eng. **44**, 1185 (2006)
2. J. Mathew, G.L. Goswami, N. Ramakrishnan, N.K. Naik, J. Mater. Process. Technol. **89–90**, 198 (1999)
3. R. Negarestani, L. Li, H.K. Sezer, D. Whitehead, J. Methven, Int. J. Adv. Manuf. Technol. **49**, 553 (2010)
4. J.P. Davim, P. Reis, Compos. Struct. **59**, 481 (2003)
5. D. Kalla, J. Sheikh-Ahmad, J. Twomey, Int. J. Mach. Tool Manu. **50**, 882 (2010)
6. I.S. Shyha, D.K. Aspinwall, S.L. Soo, S. Bradley, INT. J. Mach. Tool Manu. **49**, 1008 (2009)
7. Z.L. Li, P.L. Chu, H.Y. Zheng, G.C. Lim, L. Li, S. Marimuthu, R. Negarestani, M. Sheikh, P. Mativenga, in *Advances in Laser Materials Processing*, ed. by J. Lawrence, J. Pou, D.K.Y. Low, E. Toyserkani (Woodhead Publishing, Sawston, 2010), pp. 136–177
8. E. Uhlmann, G. Spur, H. Hocheng, S. Liebelt, C.T. Pan, Int. J. Mach. Tool Manuf. **39**, 639 (1999)
9. C.T. Pan, H. Hocheng, Compos. Part A Appl. **32**, 1657 (2001)
10. R. Negarestani, M. Sundar, M. Sheikh, P. Mativenga, L. Li, Z. Li, P. Chu, C. Khin, H. Zheng, G. Lim, Proc. Inst. Mech. Eng. Pt. B J. Eng. Manuf. **224**, 1017 (2010)
11. K.A. Fenoughty, A. Jawaid, I.R. Pashby, J. Mater. Process. Technol. **42**, 391 (1994)
12. A. Beaulieu, Appl. Phys. Lett. **16**, 504 (1970)
13. J.F. Ready, D.F. Farson, T. Feeley, *LIA Handbook of Laser Materials Processing* (Laser Institute of America, Orlando, 2001)
14. M. Forrer, M. Frenz, V. Romano, H. Altermatt, H. Weber, A. Silenok, M. Istomyn, V. Konov, Appl. Phys. B **56**, 104 (1993)
15. P. Dyer, I. Waldeck, G. Roberts, J. Phys. D Appl. Phys. **30**, L19 (1997)
16. M.S. Trtica, B.M. Gaković, T.M. Nenadović, M.M. Mitrović, Appl. Surf. Sci. **177**, 48 (2001)
17. A. Tsunemi, K. Hagiwara, N. Saito, K. Nagasaka, Y. Miyamoto, O. Suto, H. Tashiro, Appl. Phys. A Mater. **63**, 435 (1996)
18. A. Forbes, L.R. Botha, N. Du Preez, T.E. Drake, S. Afr. J. Sci. **102**, 329 (2006)
19. D. Herzog, P. Jaeschke, O. Meier, H. Haferkamp, Int. J. Mach. Tool Manu. **48**, 1464 (2008)
20. Z. Li, H. Zheng, G. Lim, P. Chu, L. Li, Compos. Part A Appl. Sci. **41**, 1403 (2010)
21. R. Negarestani, L. Li, in *Machining Technology for Composite Materials*, ed. by H. Hocheng (Woodhead Publishing, Sawston, 2012), pp. 288–308
22. A. Riveiro, F. Quintero, F. Lusquiños, J. del Val, R. Comesaña, M. Boutinguiza, J. Pou, Compos. Part A Appl. Sci. **43**, 1400 (2012)
23. C. Leone, S. Genna, V. Tagliaferri, Opt. Laser. Eng. **53**, 43 (2014)
24. R. Negarestani, L. Li, Proc. Inst. Mech. Eng. Pt. B J. Eng. Manuf. **227**, 1755 (2013)
25. J. Finger, M. Weinand, D. Wortmann, J. Laser Appl. **25**, 042007 (2013)
26. J.C. Hernández-Castañeda, H.K. Sezer, L. Li, Opt. Laser. Eng. **49**, 1139 (2011)
27. A. Ghosal, A. Manna, Opt. Laser Tech. **46**, 67 (2013)
28. A.S. Elmesalamy, L. Li, J.A. Francis, H.K. Sezer, Int. J. Adv. Manuf. Technol. **68**, 1 (2013)
29. T.A. El-Taweel, A.M. Abdel-Maaboud, B.S. Azzam, A.E. Mohammad, Int. J. Adv. Manuf. Technol. **40**, 907 (2009)
30. M.J.J. Schmidt, D.K.Y. Low, L. Li, Appl. Surf. Sci. **186**, 271 (2002)
31. S. Leigh, K. Sezer, L. Li, C. Grafton-Reed, M. Cuttell, Int. J. Adv. Manuf. Technol. **43**, 1094 (2009)
32. R. Biswas, A.S. Kuar, S. Sarkar, S. Mitra, Opt. Laser Technol. **42**, 23 (2010)
33. J.C. Hernandez-Castaneda, H.K. Sezer, L. Li, Proc. Inst. Mech. Eng. Part B J. Eng. Manuf. **223**, 775 (2009)
34. K.C. Yung, S.M. Mei, T.M. Yue, J. Mater. Process. Technol. **122**, 278 (2002)
35. C.-H. Li, M.-J. Tsai, C.-D. Yang, Opt. Laser Technol. **39**, 786 (2007)
36. A.A. Cenna, P. Mathew, Int. J. Mach. Tools Manuf. **37**, 723 (1997)
37. F.A. Al-Sulaiman, B.S. Yilbas, M. Ahsan, J. Mater. Process. Technol. **173**, 345 (2006)
38. J. Stock, M.F. Zaeh, M. Conrad, Phys. Procedia **39**, 161 (2012)
39. I. Shyha, Procedia Eng. **63**, 931 (2013)
40. T. Sumiyoshi, Y. Ninomiya, H. Ogasawara, M. Obara, H. Tanaka, Appl. Phys. A Mater. **58**, 475 (1994)
41. J. Morrison, T. Tessier, B. Gu, Circuit World **21**, 24 (1994)